Carbon 148 (2019) 336–343

Contents lists available at ScienceDirect

Carbon

journal homepage: www.elsevier.com/locate/carbon

Investigation of charges-driven interaction between graphene and different SiO_2 surfaces

Maria F. Pantano [a], Erica Iacob [b], Antonino Picciotto [b], Benno Margesin [b], Alba Centeno [c], Amaia Zurutuza [c], Costas Galiotis [d, e], Nicola M. Pugno [a, f, g, **], Giorgio Speranza [b, h, i, *]

[a] Laboratory of Bio-inspired & Graphene Nanomechanics, Department of Civil, Environmental and Mechanical Engineering, University of Trento, Via Mesiano 77, 38123, Trento, Italy
[b] Centre for Materials and Microsystems, Fondazione Bruno Kessler, Via Sommarive 18, 38123, Povo, TN, Italy
[c] GRAPHENEA S.A., Paseo Mikeletegi 83, 20009, San Sebastian, Spain
[d] Institute of Chemical Engineering Sciences, Foundation for Research and Technology – Hellas (FORTH/ICE-HT), Patras, 265 04, Greece
[e] Department of Chemical Engineering, University of Patras, Patras, 26504, Greece
[f] School of Engineering and Materials Science, Queen Mary University of London, Mile End Road, London, E1 4NS, UK
[g] Ket-Lab, Edoardo Amaldi Foundation, Via del Politecnico snc, 00133, Rome, Italy
[h] Istituto Fotonica e Nanotecnologie – CNR, via alla cascata 56, 38123, Trento, Italy
[i] Department of Material Engineering, University of Trento, Via Mesiano 77, 38123, Trento, Italy

ARTICLE INFO

Article history:
Received 11 February 2019
Received in revised form
14 March 2019
Accepted 21 March 2019
Available online 27 March 2019

Keywords:
Graphene
Silicon oxide
Surface charges
Electrostatic interaction
SKPM
Raman spectroscopy
XPS

ABSTRACT

As being only one atom thick, most of the device applications require graphene to be partially or fully supported by a substrate, which is typically silicon dioxide (SiO_2). According to a common understanding, graphene interacts with SiO_2 through weak, long-range van der Waals forces, emerging between instantaneous/induced dipoles, in contrast to the experimental evidence that reveals a surprisingly high interaction between graphene and SiO_2. In order to get further insight into this phenomenon, we carried out diverse physical measurements on SiO_2 substrates, prepared via different fabrication protocols, with and without graphene on top. As a result, the role of the oxide surface charges is recognized for the first time as a main factor causing graphene to strongly interact with SiO_2. Our findings provide guidelines for designing 2D materials interaction with a substrate through modulation of surface charges. This, in turn, can facilitate the development of new graphene based microelectronic devices.

1. Introduction

As the performances of silicon-based electronics increase with dimensional reduction, graphene has been receiving increasing attention by the scientific community. Owing to its exceptional electronic properties, which arise from the high electron mobility of carbon atoms confined in a single layer, it is likely that graphene will take a pivotal role in the future of microelectronics [1–4]. Unfortunately, graphene electrical properties are very sensitive to the interactions with the external environment. In fact, previous theoretical studies showed that the electronic states near Dirac points can be influenced by the absorption of some molecules [5,6], structural corrugation [7], defects [8] and the interaction with a substrate [9,10]. This latter condition occurs frequently in many applications. For example, graphene is commonly found as deposited onto a substrate in novel electrical switches [11], surface coatings for lubrication [12] and protection against corrosion [13], or embedded in multilayer systems as in devices for control of terahertz waves [14] and touch-panel displays [15]. In many cases a strong interaction with the substrate is required, at least at specific locations, as to securely clamp the edge of a freestanding nanoscale resonator [16] or the boundary of a membrane for mechanical tests [17–21] or to induce strain through a flexible substrate in order to investigate strain engineering properties [22]; whereas in many

* Corresponding author. Centre for Materials and Microsystems, Fondazione Bruno Kessler, Via Sommarive 18, 38123, Povo, TN, Italy.
** Corresponding author. Laboratory of Bio-inspired & Graphene Nanomechanics, Department of Civil, Environmental and Mechanical Engineering, University of Trento, Via Mesiano 77, 38123, Trento, Italy.
E-mail addresses: nicola.pugno@unitn.it (N.M. Pugno), speranza@fbk.eu (G. Speranza).

https://doi.org/10.1016/j.carbon.2019.03.071
0008-6223/

others the interaction should be as low as possible, as in electromechanical switches, or of medium intensity, in order to have well-adhered but sliding graphene flakes able to fold in nanoribbons [23].

Thus, a deep understanding of the mechanism behind the interaction of graphene with a substrate is not only interesting from a fundamental point of view but becomes necessary when applications in electronics are considered. Unfortunately, the origin of such interaction still remains an open question and a satisfactory explanation still lacks [24] in spite of a number of both numerical [10,25,26] and experimental [27–30] studies.

The investigated substrate materials span over metals, like Ni and Cu [29], to silicon oxide, a common insulator in electronic devices. The first measurement of the adhesion energy of a monolayer graphene on SiO_2 revealed a surprisingly high interaction, which was ascribed to the graphene ability to conform in a liquid-like fashion over even smooth surfaces [28]. According to a common understanding, the interaction of graphene with SiO_2 is believed to be controlled by weak, long-range van der Waals forces, emerging between instantaneous/induced dipoles forming in either graphene or SiO_2 [31,32]. A similar mechanism is known to determine also the adhesion of micromachined surfaces [33]. However, it was recently demonstrated by multiscale modeling [31] that van der Waals forces alone cannot explain the high tensile and shear toughness of graphene/SiO_2 interface as found in adhesion experiments. As an alternative explanation, was adduced the possible role played by surface defects, such as undercoordinated Si atoms and non-bridging O atoms, to which graphene can bind. As a matter of fact, no sufficient attention has ever been paid to the presence of charges either within the oxide layer or located at its surface that can strongly interact with graphene. Nevertheless, it is well known in microelectronics that the growth of oxide on top of Si wafers causes residual charges to develop at the interface [34]. In addition, SiO_2 surface is known to be rich of silanol groups (Si-OH). These originate from the interaction of silica with water molecules in air and commonly undergo protonation reactions [35], which leave significant surface charges.

Thus, in the present work we explore how such charge sources can be responsible for the strong interaction of graphene with SiO_2-based substrates.

2. Experimental

2.1. Silicon substrates preparation

In order to highlight the role of surface charges of SiO_2 in its interaction with graphene, we considered a number of Si/SiO_2 substrates with different amount of superficial charge. These substrates were fabricated by varying three main parameters, namely, the silicon crystal orientation (a), the oxide growth process (b) and the thermal treatment after the oxide formation (c). With reference to the first parameter (a), rectangular slices were cut from either a Si 111 wafer or non-crystalline Quartz wafer. Then, (b) three types of oxide were considered. The first is the native oxide (NO), which naturally grows from the exposure of a Si wafer to air. The other two oxides (300 nm thick in both cases) were obtained by either thermal growth through direct oxidation of a Si 111 wafer (thermal oxide, TO) or deposition from a tetraethylorthosilicate precursor (TEOS). (c) After oxide deposition/growth, some samples with either TO or TEOS oxide were annealed at 950 °C for 30 min in N_2 atmosphere (TO+AN and TEOS+AN, respectively). The last type of sample was derived from a Si 111 wafer where a thin layer (in the range of 5–10 nm) of CH_4+H_2 was deposited after HF etching the native oxide. The variation of the previous three process parameters implied the availability of 7 different substrates, and on each of them a monolayer graphene was transferred. More details about the Si samples preparation can be found in the Supporting Information.

2.2. Graphene preparation

Monolayer graphene samples were grown using a copper (Cu) foil catalyst by Chemical Vapor Deposition (CVD). Graphene synthesis was carried out in a cold walled CVD reactor (Aixtron BM) at 1000 °C and at low pressure using methane as the carbon source. Prior to the growth, the Cu foils were chemically treated in order to clean and smoothen the surface followed by annealing at 1000 °C under hydrogen and argon flow. After the synthesis, a poly(methyl methacrylate) (PMMA) sacrificial support layer was spin coated onto the graphene covered Cu foil. Cu was chemically etched using a ferric chloride containing solution followed by different cleaning steps in distilled water and acid solutions. The monolayer graphene was transferred onto different substrates. The film was dried at 120 °C for few hours and finally, the PMMA layer was removed by dipping into acetone and IPA.

2.3. Raman spectroscopy

Raman measurements were carried out on a LabRAM Aramis (HORIBA Jobin Yvon, France, with a 632.8 nm laser at a magnification of 50x and a 1200 grooves/mm grating. Spectra were acquired with an integration time of 5s repeated twenty times. The data reported refer to the mean of 6 measurements at different locations on the same sample. Before the analysis, all the samples were cleaned by thermal annealing at 500 °C for 1 h with the only exception of Si covered with CH_4+H_2, which would receive severe damage from the high temperature treatment.

2.4. Amplitude Modulation-Scanning Kelvin Probe Microscopy

Here, we used an Atomic Force Microscope (AFM) named Solver Px by NT-MDT. AFM topographical data were acquired in semicontact mode while the surface potential was measured using the Amplitude Modulation-Scanning Kelvin Probe Microscopy (AM-SKPM). SKPM is a two-pass technique. After the topographical scan (which resulted to be the same in both trace and retrace) the tip was lifted up 10 nm off the sample surface and the surface potential data were acquired at a fixed distance from the sample surface. We used noncontact high resolution silicon cantilevers NSG10 series with PtIr conductive coating. The thickness of the coating is 20–30 nm and the typical tip curvature radius is 35 nm. Tips were electrically calibrated against fresh exfoliated graphite. The results reported in the manuscript are obtained from repeated analyses made on different samples whose number depends on the signal variability. For TO, the data refers to the average of 9 mean contact potential difference (CPD) values- each referring to a random region of few tens μm^2 area- made in different days. For TO + AN and NO samples the data refers to an average of 5 mean CPD values- each referring to a random region of few tens μm^2 area- made in different days. For TEOS and TEOS + AN samples the data refers to an average of 4 and 5, respectively, mean CPD values- each referring to a random region of few tens μm^2 area- made in different days. For CH_4+H_2 sample the variability was very low and the reported data refer to an average of 2 mean CPD values- each referring to a random region of few tens μm^2 area- made on the same day. Different quartz samples were measured in different days but the variability was always too large to provide enough statistical significance.

2.5. XPS analysis

The Axis Ultra XPS spectrometer by Kratos, UK, was calibrated with respect to the Au 4f 7/2 peak position fixed at 84.00 eV for a polycrystalline Au foil. The Fermi-level position was then obtained considering the inflection point of the signal intensity on the Au Fermi Edge following the procedure of the instrument manufacturer. Spectra were acquired using a pass energy of 80 eV and an energy step of 0.1eV. 20 sweeps were acquired for each of the Valence Band spectra to obtain a good signal-to-noise ratio.

3. Results and discussion

In order to characterize the interaction of graphene with each substrate, Raman spectroscopy was employed. Although Raman spectroscopy is generally used to assess the quality of graphene based films, it can also be effectively employed for the evaluation of substrate/graphene interactions [36]. Indeed, as it probes the vibrational states of a system of atoms, Raman spectroscopy is sensitive to an even minimum modification of their electronic structure [37,38], including the doping level [39] and the interaction with exogeneous chemical species. For example, it has been demonstrated that oxygen molecules adsorbed on SiO_2 are able to interact with the aromatic rings of graphene thus modifying its charge distribution [40–43].

The vibrational mode characteristics (eg peak position and bandwidth) are also sensitive to the application of stress or strain from the environment or substrate. This suggests that in our case the effect of a different preparation of our SiO_2 surfaces should induce detectable changes in the Raman spectra of graphene depending on the strength of its interaction with the substrate [44,45]. Similar indications are given by both theoretical [10,46] and experimental works [36,47]. Indeed, the Raman spectra of our samples differ from one another in many respects, such as the position and broadening of the graphene characteristic G and 2D peaks, as well as their relative intensity (Fig. 1a, Figure S1 and Table S1). Let us first consider the positions of the G and 2D peaks (Fig. 1b).

As stated before, a shift of the Raman peaks can be related to different factors, mainly including the doping and the strain that can be induced, even uncontrollably, during the fabrication process. In fact, even if the samples are prepared according to the same protocol, as in our case, still differences may arise. In order to deconvolute the mechanical contribution to the Raman shift from that due to the electrical charges in graphene, it is useful to study the relative position of the G and 2D peaks across our samples. According to a previously reported methodology [48], in the G frequency-2D frequency plane, it is possible to identify two reference lines that represent graphene samples showing either no doping or no strain (blue and red lines in Fig. 2, respectively). The intersection of these two lines defines a reference point *O* with coordinates (1581.6; 2676.9) cm^{-1} corresponding to a sample with zero strain and zero charge. Interestingly, if we plot the Raman 2D frequencies against the G frequencies of all our samples, we can draw about 40 data points that result to be well aligned. Considering a regression fit, the slope of the fitting line is 0.89 that is much smaller than the charge free line, whose slope is reported as 2.02–2.44 [48], yet it matches very well the slope of the free strain line that is reported to be 0.75 ± 0.04 [48]. From this evidence, we can reasonably state that no significant difference in strain can be observed across our samples. This same conclusion emerges if we compute and compare the strain of each sample as follows. For each point representing our samples we can draw a line - parallel to the free strain line - whose intersection with the free charge line defines a new point with an associated G frequency. Its frequency shift, $\Delta\omega_G$, from the reference point *O* allows to estimate the corresponding hydrostatic strain, ε_h, as [49]:

$$\varepsilon_h = - \Delta\omega_G / \omega_0 \gamma \quad (1)$$

where ω_0 is the G frequency of the reference point *O* and γ is the Grüeneisen parameter equal to 1.8 [49] (more details can be found in the SI). Overall, the mean hydrostatic strain, $\varepsilon_h = \varepsilon_{xx} + \varepsilon_{yy}$, across all the samples is $1.0\% \pm 0.1\%$. If we assumed a biaxial strain, ε_b, on our graphene samples, this would be half of the computed hydrostatic strain, i.e. $\varepsilon_b = \varepsilon_{xx} = \varepsilon_{yy} = 0.5\%$. Such value matches very well the strain due to friction of water when a graphene sheet is deposited through wet transfer on a Si substrate as it was in our case (more details in the SI).

Then, since no significant difference in strain can be observed, we can argue that the main factor causing the shift of the Raman peaks from one sample to the other is the presence of charges in graphene. Furthermore, from the same G-2D frequencies plot and following the same approach considered previously in the case of the strain, we can derive the amount of charge affecting each sample, too. In particular, since the sensitivity of the 2D peak

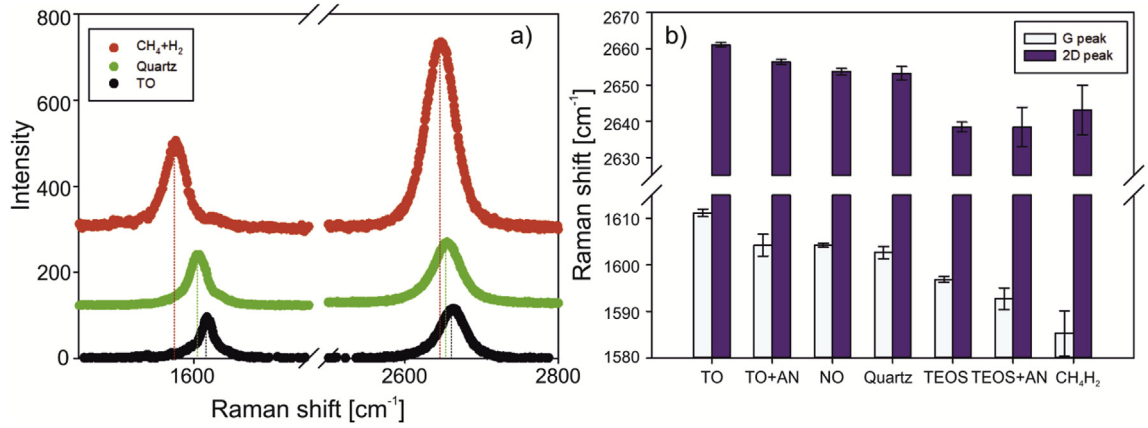

Fig. 1. a) Raman spectra of graphene transferred on a Si 111 wafer with thermal oxide on top (TO), Quartz and Si 111 with a thin layer of CH_4+H_2 (aC:H) deposited on top after etching its native oxide. A blue-shift of both G and 2D peaks is visible when graphene is on either Quartz or TO with respect to graphene on Si111 with CH_4+H_2 layer. b) Position of the G and 2D peaks of Raman spectra recorded for graphene on different Silicon-based substrates: Si 111 with thermal oxide on top (Si), Si 111 with annealed thermal oxide (TO+AN), Si 111 with native oxide (NO), Quartz, Si 111 with TEOS oxide (TEOS), Si 111 with annealed TEOS oxide (TEOS+AN), Si 111 with a thin layer of CH_4+H_2 deposited after etching of Si native oxide with HF (CH_4H_2). (A colour version of this figure can be viewed online.)

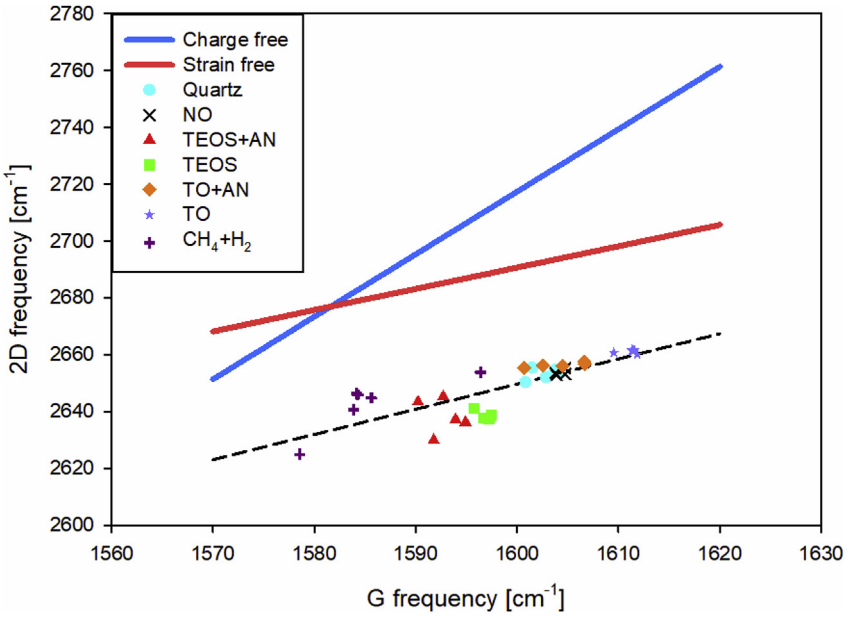

Fig. 2. Frequency of the 2D peak vs the frequency of the G peak of a monolayer graphene deposited on different silicon substrates. The experimental points can be fitted by a line (dashed in the plot) that results to be almost parallel to the reference line corresponding to a graphene sample with no strain (strain free line in red). (A colour version of this figure can be viewed online.)

frequency against the number of charges for unit area is about 0.7 $x10^{-12}$ (1 $x10^{-12}$) cm^2/cm [35,50], from the projection of the border points along the free strain axis, we can find that the amount of charge across our samples vary between 3.2 (2.2) $x10^{13}$ cm^{-2} (graphene on Si with a CH_4+H_2 layer) and 6.0 (4.2) $x10^{13}$ cm^{-2} (graphene on Si with TO on top). More details about such estimation are reported in the SI.

Overall, a difference of about 2.7 (1.9) $x10^{13}$ cm^{-2} charge density across our samples causes a blue shift of the G frequency of up to 26 cm^{-1} that is then comparable with the concentration of electrons/holes able to cause a 21 (17) cm^{-1} blue shift of the Raman G peak as previously reported [38].

Both the values of strain and doping that we derived depend on the slope of the zero charge and zero strain lines. However, while in the case of the zero-charge line there is a good agreement in the literature, more uncertainties still affect the estimation of the zero strain line with reported values in the range 0.55 ± 0.2–0.75 ± 0.05 [38,48,51].

It is now interesting to explore the origin of the different doping level across our graphene samples. It was recently reported that in the case of a strong interaction with an external charge (distribution), as in our case [52,53], graphene behaves like a metal where the external charge distribution induces the development of image charges [53]. As a consequence, we can argue that since our graphene samples are always deposited onto polar SiO_2 surfaces, they develop an image charge that matches in magnitude that of the underlying SiO_2 [53]. Thus, differences in the graphene charge, as revealed by the analysis of Raman spectra, are to be ascribed to variations in the charges amount of our SiO_2 substrates. The sample showing the highest blue shift (e.g., highest charge amount) corresponds to graphene deposited on Si with thermal oxide on top, whereas the sample with the lowest blue shift corresponds to Si with a CH_4+H_2 layer. In between, there are those with either TEOS oxides (TEOS and TEOS + AN). The observed differences can be explained considering the process used to fabricate the Si oxide layer. In the case of TO type, the growth of the thermal oxide proceeds at the expense of the underlying Si wafer, thus inducing a distortion of the Si crystal lattice at the interface. Such a distortion is accompanied by the formation of a residual electrical charge (that can be estimated as $<10^{12}$ cm^{-2} [54]). However, this residual charge is much more limited than that of TEOS, where the quality of the oxide is lower and characterized by the presence of a charge density of ~10^{12} cm^{-2}. A method commonly used in electronics to reduce such a charge density is annealing at high temperatures (950 °C), which induces a relaxation of the inner strains and a reduction of the charge to ~10^{10} cm^{-2}. Thus, in the hypothesis of electrostatic interaction between graphene and the substrate, we expect that a thermal process would reduce the intensity of their interaction. Indeed, this explains why the blue shift of G (2D) peak for a given substrate is lower when thermal annealing is introduced. Furthermore, as a limiting case, the absence of the oxide layer (e.g., the native oxide is etched and the underlying substrate is covered with a CH_4+H_2 layer) should provide the smallest amount of residual charge, which, in turn, should provide the lowest graphene interaction. As a confirmation, the CH_4+H_2 substrate provides the most red-shifted G peak in the Raman spectra. However, if we consider only the amount of charge embedded in the oxide layer, we could not explain why TO substrates provide more interaction than TEOS substrates (Fig. 1b). Indeed, apart from the charge embedded in the oxide, it is well known that SiO_2 interacts with water (even in ambient conditions) with the formation of silanol groups on its surface. Such groups are then subjected to protonation reactions [35] that cause the formation of an even significant amount of surface charge (up to 10^{14} cm^{-2}), which is much higher than the residual interface charge [54,55]. Overall, the amount of surface charge expected on SiO_2 as a consequence of both the fabrication process and protonation reactions is compatible with the estimation derived from the analysis of the Raman spectra. Other evidences of the presence of charges in graphene come from an analysis of the FWHM of the G peak. In a previous study [38] it was shown that the FWHM significantly decreases when the number of charges in graphene increases up to 5 x 10^{12} cm^{-2}. Then, it stabilizes within the range 6 cm^{-1} – 11 cm^{-1}. Interestingly, this is the same interval that includes the G peak FWHM of all our samples

(Table S1), which thus results to be compatible with the presence of few 10^{13} cm^{-2} charges as we identified from the G (2D) frequency shift. Similarly, the relative intensity of the 2D and G peak, I_{2D}/I_G, decreases significantly when the number of charges in graphene increases up to 5 x 10^{12} cm^{-2}. Then, the reduction trend is much less pronounced and for a number of charge bigger than 5 x 10^{12} cm^{-2}, I_{2D}/I_G was reported to be smaller than 1.5 [38], which matches our experimental evidence (Table S1). The only I_{2D}/I_G slightly bigger in our experiments (1.65 ± 0.76) was recorded for the CH_4+H_2 sample, which has the smallest amount of electrical charge, though.

In order to confirm that the strong interaction of graphene and SiO_2 is related to the amount of surface charges of our Si/SiO_2 substrates, we measured the surface potential of these latter through AM-SKPM. AM-SKPM is a non-contact method for direct measurement of the contact potential difference (CPD) between an AFM tip and a sample surface [56] (Fig. 3a). Since the CPD between two materials depends on a variety of parameters, such as the work function [57] and dopant concentration in semiconductors [58], this can provide information about the whole surface charge, including both the contributions of the embedded charge and the charge due to polar groups on the substrate surface [59]. For the quantitative measurement of CPD distribution, before the experiments, the tip of the SKPM was first calibrated against fresh exfoliated graphite (HOPG) and then used to scan each substrate in order to have a map of its topography and surface potential (Fig. 3b–c). The surface potential of each substrate, V_s, was evaluated according to the following equation:

$$V_s = CPD + V_T \quad (2)$$

where *CPD* is measured directly by the instrument and V_T is the tip surface potential. This latter can be computed as V_{HOPG}-CPD_{cal}, where CPD_{cal} is the contact potential distribution measured by the instrument during the tip calibration and V_{HOPG} is the HOPG surface potential, assumed here equal to 4.475 V [60].

Fig. 3d reports the surface potential of each substrate directly measured by SKPM as compared to the charge density of the corresponding graphene sample on top derived from the interpretation of the Raman spectra according to the previously discussed procedure. Surprisingly, the variations of the surface potential and graphene charge density across the different substrates are in

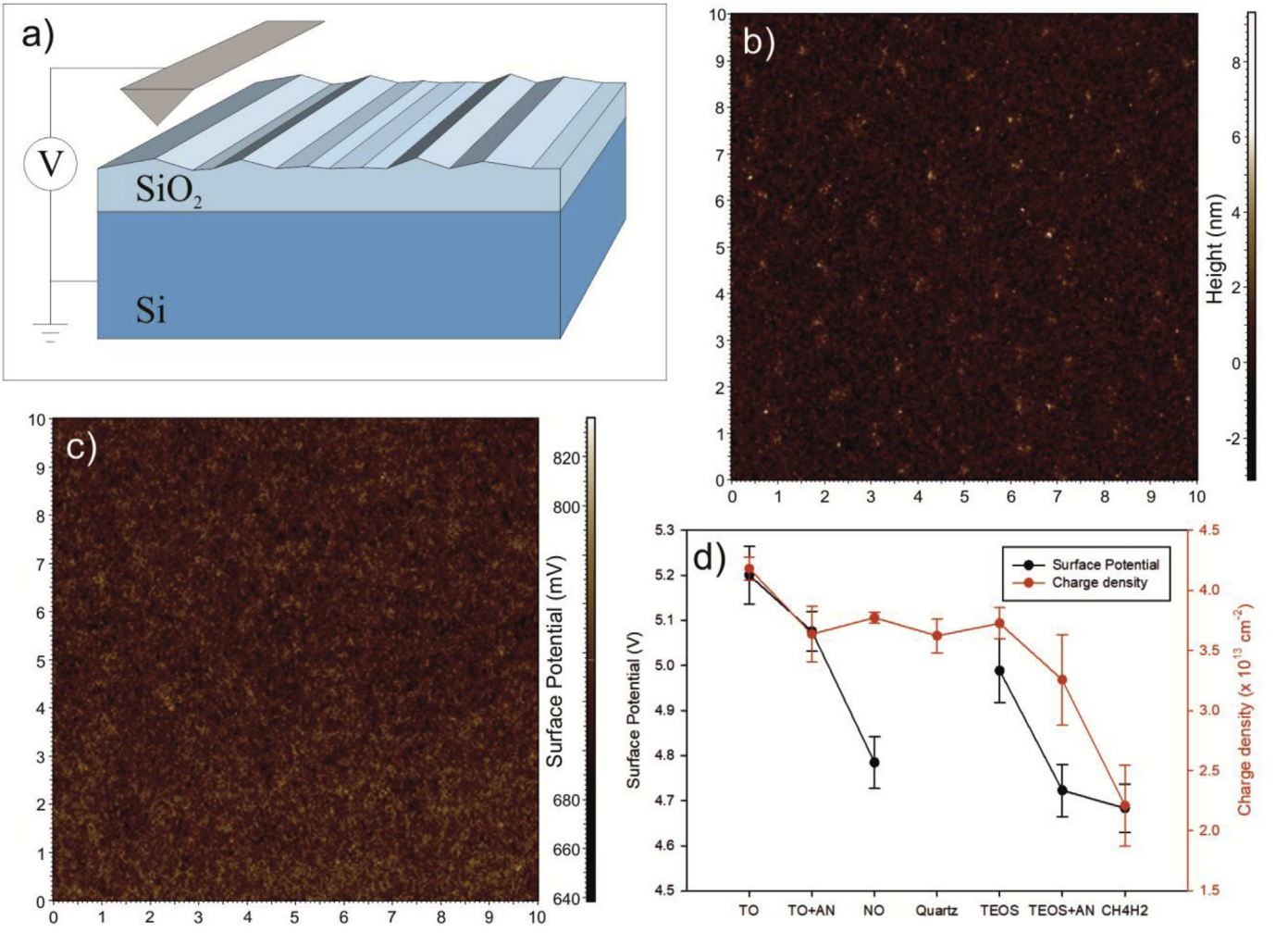

Fig. 3. a) Surface potential measurement setup. During the measurement, each Si/SiO_2 substrate is grounded. b) Example topographical and (c) surface potential maps derived from the SKPM tip scanning a 10×10 μm^2 sample surface area. Before the electrical measurement, the SKPM tip was calibrated against a reference graphite sample; d) Comparison of the surface potential measured for different Si substrates (Si 111 with thermal oxide (TO), Si 111 with thermal oxide treated with thermal annealing (TO+AN), Si 111 with native oxide (NO), quartz, Si 111 with TEOS oxide, Si 111 with TEOS oxide treated with thermal annealing (TEOS+AN), Si 111 with a thin layer of CH_4H_2 deposited after etching its native oxide with HF) and expressed as absolute difference with respect to graphite work function. The surface potential data are compared to the charge density evaluated from the Raman spectra of a graphene sheet deposited on each of the considered substrates. (A colour version of this figure can be viewed online.)

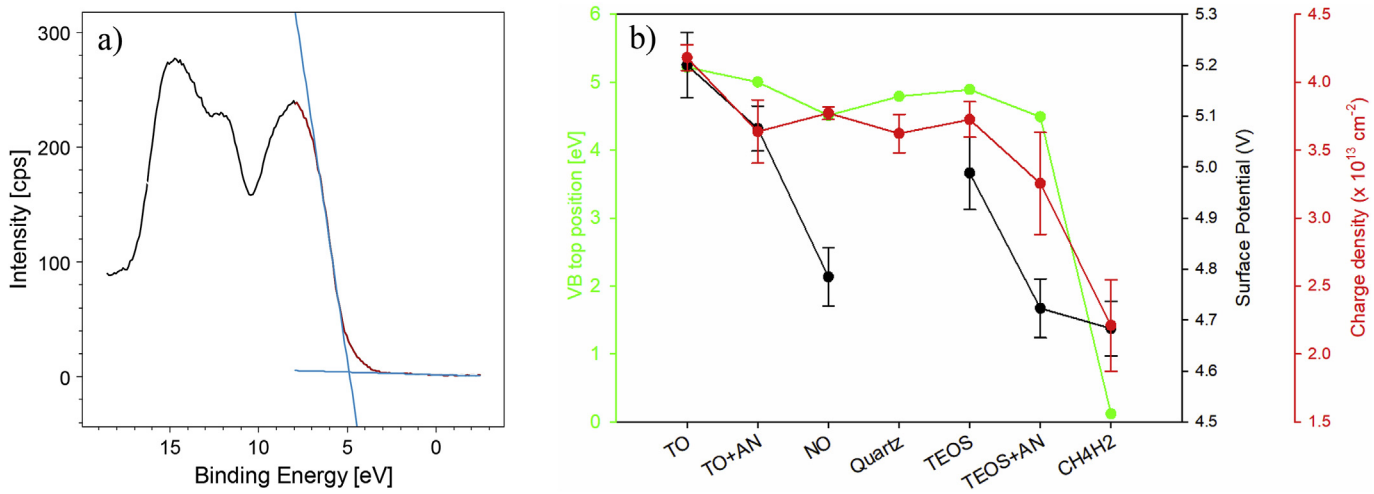

Fig. 4. a) Valence Band (VB) of a TEOS sample derived from XPS measurement. According to a conventional linear fit algorithm, the top of the VB is determined as the intersection between the linear fit of the falling shoulder of the VB and the VB background above the Fermi level; b) Position of the Valence band Top estimated for different Si based substrates: Si 111 with thermal oxide on top, Si 111 with thermal oxide on top and treated with thermal annealing, Si 111 with native oxide, quartz, Si 111 with TEOS oxide, Si 111 with TEOS oxide and treated with thermal annealing, Si 111 with a thin layer of CH_4+H_2 deposited after etching its native oxide with HF. (A colour version of this figure can be viewed online.)

general agreement with one another, despite they refer to different physical entities measured through different techniques. Some differences can be noted only in the case of NO and CH_4+H_2 and these can be explained by the same reason, though. Indeed, both the samples consist of a few nanometers thick layer laying on a bulk silicon substrate. From the literature it is well known that SKPM can reach a depth sensitivity of several hundreds of nanometers, which enables it to detect objects located beneath the scanned surface [61]. Thus, it is very likely that the CPD measured in our SKPM tests takes into account not only the surface potential strictly related to the thin film of interest, but also the substrate contribution. In addition, this contribution affects differently NO and CH_4+H_2. In the first case, since Si has higher conductivity than NO, we expect that the substrate presence causes a reduction of the measured surface potential (i.e., the corresponding value reported in Fig. 3d is underestimated). On the contrary, in the second case, as the CH_4+H_2 film is more conductive than Si, we expect an overestimation of the measured CPD (i.e., the actual value is smaller than the reported one). The relatively high depth sensitivity of SKPM explains also the unavailability of stable data for quartz, which is not reported in Fig. 3d, with respect the other substrates. In fact, the experimental condition for the SKPM measurement on quartz involves testing of a 600 μm thick bulk sample, whereas in all the other cases, the tested samples consist of oxide layers of at least 300 nm thickness laying on a bulk Si substrate connected to the ground. Since the SKPM tip has a relatively high depth sensitivity, the presence of the bulk Si played a beneficial role in stabilizing the measurement on the upmost oxide layer. On the contrary, in the case of quartz, the surface to be tested belongs to a bulk dielectric material, which is not possible to ground. This causes the electrical measurement to be unstable and thus not reliable.

Finally, in order to have the ultimate evidence that there is a difference in the amount of surface dipoles across our substrates, we performed XPS analysis. This allows for an estimation of the Valence Band top (VB-top) position, which is in turn sensitive to the surface charge distribution caused by dipoles.

In oxidized silicon samples, a negative surface charge is expected due to the charge transfer from silicon to oxygen in positively doped samples as ours. Negative charges induce a downward band bending that increases the distance between the VB-top and the Fermi level [62,63]. The opposite occurs when positive charges accumulate on the sample surface that lead instead to an upward band bending. Since in our analysis, the Fermi level was carefully aligned to zero utilizing a polycrystalline sputtered gold sample, the differences in the VB-top result from the different surface composition. In particular, the higher the band bending the more negative the surface charge. Alternatively, we can say that the higher the potential measured by the SKPM, the higher the regression of the VB-top from the Fermi level due to band bending.

Indeed, we find a good agreement between the trend of the band bending induced by the charge accumulation on the sample surface with the surface potential measured by SKPM (Fig. 4b) and the graphene charge density previously estimated through Raman spectroscopy. In this regard, the only slight outlier is the NO sample. However, in this latter case the estimation of VB-top position was more complex as a consequence of additional features of NO valence band with respect to the other samples (see Figs. 4a and 5). Indeed, we observed a shoulder near the Fermi edge which can be

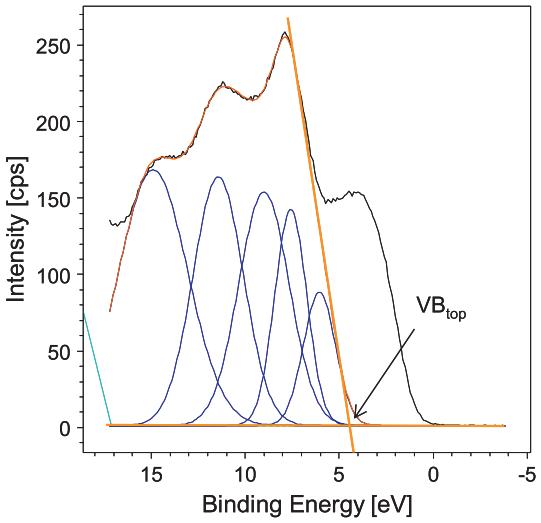

Fig. 5. Valence band (VB) of an example Si 111 sample with a native oxide layer on top and evaluation of the VB-top after eliminating the contribution of bulk Si. (A colour version of this figure can be viewed online.)

assigned to a non-negligible density of states near the Fermi edge due to the semiconducting nature of the underlying bulk Si substrate, as already described in the literature by experimental and theoretical works [64–67]. Differently from the other samples, in this case we are sensitive to the bulk Si because the native oxide layer is very thin and in particular it is thinner than the sampling depth of the X-rays for photoelectrons at ~1480 eV.

To estimate the position of the VB-top in the case of the NO sample, the contribution of the silicon substrate was firstly eliminated through a Gaussian fitting procedure (see SI) and then the top of the valence band was evaluated through a linear fit as for the other samples (Fig. 5). Our estimation of 4.51eV results in very good agreement with data reported in literature [65], but an underestimation with respect to the other samples cannot be excluded because of the required additional analysis.

4. Conclusions

In this work the interaction between graphene and SiO_2 was proven to be related to the electrical charges at the SiO_2 surface originating from both the oxide fabrication process and protonation reactions. This clue results from experimental evidences obtained through different and independent physical techniques including Raman spectroscopy, Scanning Kelvin Probe Microscopy and X-ray Photoelectron Spectroscopy.

Raman analyses performed on graphene monolayers deposited onto different oxidized Si substrates obtained by induced oxidation or by deposition of silica from TEOS, revealed that each sample interacts with its substrate through an electrostatic interaction which depends on the amount of surface charges. The presence of a varying surface charge across our substrates was also confirmed by both SKPM, through a direct measurement of their surface potential, and XPS analyses, through an estimation of their valence band bending. Interestingly, the SiO_2/Si substrates characterized by higher/lower charge correspond to higher/lower interaction with graphene. Our results indicate that substrate surface charges, if properly controlled, may enable tuning the graphene and 2D materials interaction with different substrates. Such mechanism can open new frontiers in microelectronics and can then be exploited in novel multifunctional devices providing strong adhesion only at particular locations and for even large areas.

Acknowledgements

The authors wish to thank Dr. Konstantinos Papagelis and Nick Delikoukos for deposition of graphene on NO and quartz substrates.

NMP and CG are supported by the European Commission H2020 under the Graphene Flagship Core 2 No. 785219 (WP14 “Composites”). NMP is also supported by the European Commission H2020 under the FET Proactive “Neurofibres” Grant No. 732344 as well as by the Italian Ministry of Education, University and Research (MIUR) under the “Departments of Excellence” grant L.232/2016.

AC and AZ are supported by European Commission under the Graphene Flagship (WP15 ′Production).

Appendix A. Supplementary data

Supplementary data to this article can be found online at https://doi.org/10.1016/j.carbon.2019.03.071.

References

[1] A.C. Ferrari, F. Bonaccorso, V. Fal'ko, K.S. Novoselov, S. Roche, P. Boggild, S. Borini, F.H.L. Koppens, V. Palermo, N. Pugno, J.A. Garrido, R. Sordan, A. Bianco, L. Ballerini, M. Prato, E. Lidorikis, J. Kivioja, C. Marinelli, T. Ryhanen, A. Morpurgo, J.N. Coleman, V. Nicolosi, L. Colombo, A. Fert, M. Garcia-Hernandez, A. Bachtold, G.F. Schneider, F. Guinea, C. Dekker, M. Barbone, Z. Sun, C. Galiotis, A.N. Grigorenko, G. Konstantatos, A. Kis, M. Katsnelson, L. Vandersypen, A. Loiseau, V. Morandi, D. Neumaier, E. Treossi, V. Pellegrini, M. Polini, A. Tredicucci, G.M. Williams, B. Hee Hong, J.-H. Ahn, J. Min Kim, H. Zirath, B.J. van Wees, H. van der Zant, L. Occhipinti, A. Di Matteo, I.A. Kinloch, T. Seyller, E. Quesnel, X. Feng, K. Teo, N. Rupesinghe, P. Hakonen, S.R.T. Neil, Q. Tannock, T. Lofwander, J. Kinaret, Science and technology roadmap for graphene, related two-dimensional crystals, and hybrid systems, Nanoscale 7 (2015), https://doi.org/10.1039/C4NR01600A, 4598–4810.

[2] A.K. Geim AK, K.S. Novoselov, The rise of graphene, Nat. Mater. 6 (2007) 183–191.

[3] D. Jariwala, T.J. Marks, M.C. Hersam, Mixed-dimensional van der Waals heterostructures, Nat. Mater. 16 (2016) 170–181, https://doi.org/10.1038/nmat4703.

[4] R. Dong, L. Moore, L.E. Ocola, I. Kuljanishvili, Enabling quality interfaces with mask-free approach to selective growth of MoS2/graphene stacked structures, Adv. Mater. Interfaces 3 (2016) 1600098.

[5] T.O. Wehling, K.S. Novoselov, S.V. Morozov, E.E. Vdovin, M.I. Katsnelson, A.K. Geim, A.I. Lichtenstein, Molecular doping of graphene, Nano Lett. 8 (2008) 173–177, https://doi.org/10.1021/nl072364w.

[6] X. Fan, L. Liu, J.-L. Kuo, Z. Shen, Functionalizing single- and multi-layer graphene with Br and Br $_2$, J. Phys. Chem. C 114 (2010) 14939–14945, https://doi.org/10.1021/jp1041537.

[7] D.C. Elias, R.R. Nair, T.M.G. Mohiuddin, S.V. Morozov, P. Blake, M.P. Halsall, A.C. Ferrari, D.W. Boukhvalov, M.I. Katsnelson, A.K. Geim, K.S. Novoselov, Control of graphene's properties by reversible hydrogenation: evidence for graphane, Science 323 (2009) 610–613, https://doi.org/10.1126/science.1167130.

[8] J.-H. Kim, J.H. Hwang, J. Suh, S. Tongay, S. Kwon, C.C. Hwang, J. Wu, J. Young Park, Work function engineering of single layer graphene by irradiation-induced defects, Appl. Phys. Lett. 103 (2013) 171604, https://doi.org/10.1063/1.4826642.

[9] Y.-J. Kang, J. Kang, K.J. Chang, Electronic structure of graphene and doping effect on SiO 2, Phys. Rev. B 78 (2008), https://doi.org/10.1103/PhysRevB.78.115404.

[10] X.F. Fan, W.T. Zheng, V. Chihaia, Z.X. Shen, J.-L. Kuo, Interaction between graphene and the surface of SiO $_2$, J. Phys. Condens. Matter 24 (2012) 305004, https://doi.org/10.1088/0953-8984/24/30/305004.

[11] J. Bai, X. Zhong, S. Jiang, Y. Huang, X. Duan, Graphene nanomesh, Nat. Nanotechnol. 5 (2010) 190–194, https://doi.org/10.1038/nnano.2010.8.

[12] K.-S. Kim, H.-J. Lee, C. Lee, S.-K. Lee, H. Jang, J.-H. Ahn, J.-H. Kim, H.-J. Lee, Chemical vapor deposition-grown graphene: the thinnest solid lubricant, ACS Nano 5 (2011) 5107–5114, https://doi.org/10.1021/nn2011865.

[13] D. Prasai, J.C. Tuberquia, R.R. Harl, G.K. Jennings, K.I. Bolotin, Graphene: corrosion-inhibiting coating, ACS Nano 6 (2012) 1102–1108, https://doi.org/10.1021/nn203507y.

[14] S.H. Lee, M. Choi, T.-T. Kim, S. Lee, M. Liu, X. Yin, H.K. Choi, S.S. Lee, C.-G. Choi, S.-Y. Choi, X. Zhang, B. Min, Switching terahertz waves with gate-controlled active graphene metamaterials, Nat. Mater. 11 (2012) 936–941, https://doi.org/10.1038/nmat3433.

[15] G. Anagnostopoulos, P.-N. Pappas, Z. Li, I.A. Kinloch, R.J. Young, K.S. Novoselov, C.Y. Lu, N. Pugno, J. Parthenios, C. Galiotis, K. Papagelis, Mechanical stability of flexible graphene-based displays, ACS Appl. Mater. Interfaces 8 (2016) 22605–22614, https://doi.org/10.1021/acsami.6b05227.

[16] J.S. Bunch, A.M. van der Zande, S.S. Verbridge, I.W. Frank, D.M. Tanenbaum, J.M. Parpia, H.G. Craighead, P.L. McEuen, Electromechanical resonators from graphene sheets, Science 315 (2007) 490–493, https://doi.org/10.1126/science.1136836.

[17] J.S. Bunch, S.S. Verbridge, J.S. Alden, A.M. van der Zande, J.M. Parpia, H.G. Craighead, P.L. McEuen, Impermeable atomic membranes from graphene sheets, Nano Lett. 8 (2008) 2458–2462, https://doi.org/10.1021/nl801457b.

[18] C. Lee, X. Wei, J.W. Kysar, J. Hone, Measurement of the elastic properties and intrinsic strength of monolayer graphene, Science 321 (2008) 385–388, https://doi.org/10.1126/science.1157996.

[19] G.-H. Lee, R.C. Cooper, S.J. An, S. Lee, A. van der Zande, N. Petrone, A.G. Hammerberg, C. Lee, B. Crawford, W. Oliver, J.W. Kysar, J. Hone, High-strength chemical-vapor-deposited graphene and grain boundaries, Science 340 (2013) 1073–1076, https://doi.org/10.1126/science.1235126.

[20] J.-U. Lee, D. Yoon, H. Cheong, Estimation of young's modulus of graphene by Raman spectroscopy, Nano Lett. 12 (2012) 4444–4448, https://doi.org/10.1021/nl301073q.

[21] M.F. Pantano, G. Speranza, C. Galiotis, N. Pugno, A mechanical system for tensile testing of supported films at the nanoscale, Nanotechnology 29 (2018) 395707, https://doi.org/10.1088/1361-6528/aacf50.

[22] S. Deng, A.V. Sumant, V. Berry, Strain engineering in two-dimensional nanomaterials beyond graphene, Nano Today 22 (2018) 14–35, https://doi.org/10.1016/j.nantod.2018.07.001.

[23] J. Annett, G.L.W. Cross, Self-assembly of graphene ribbons by spontaneous self-tearing and peeling from a substrate, Nature 535 (2016) 271–275, https://doi.org/10.1038/nature18304.

[24] J.S. Bunch, M.L. Dunn, Adhesion mechanics of graphene membranes, Solid State Commun. 152 (2012) 1359–1364, https://doi.org/10.1016/j.ssc.2012.04.029.

[25] Y. He, W.F. Chen, W.B. Yu, G. Ouyang, G.W. Yang, Anomalous interface

adhesion of graphene membranes, Sci. Rep. 3 (2013), https://doi.org/10.1038/srep02660.
[26] W. Gao, P. Xiao, G. Henkelman, K.M. Liechti, R. Huang, Interfacial adhesion between graphene and silicon dioxide by density functional theory with van der Waals corrections, J. Phys. Appl. Phys. 47 (2014) 255301, https://doi.org/10.1088/0022-3727/47/25/255301.
[27] P. Gong, Q. Li, X.Z. Liu, R.W. Carpick, P. Egberts, Adhesion mechanics between nanoscale silicon oxide tips and few-layer graphene, Tribol. Lett. 65 (2017) 61–75.
[28] S.P. Koenig, N.G. Boddeti, M.L. Dunn, J.S. Bunch, Ultrastrong adhesion of graphene membranes, Nat. Nanotechnol. 6 (2011) 543–546, https://doi.org/10.1038/nnano.2011.123.
[29] S. Das, D. Lahiri, D.-Y. Lee, A. Agarwal, W. Choi, Measurements of the adhesion energy of graphene to metallic substrates, Carbon 59 (2013) 121–129, https://doi.org/10.1016/j.carbon.2013.02.063.
[30] Z. Zong, C.-L. Chen, M.R. Dokmeci, K. Wan, Direct measurement of graphene adhesion on silicon surface by intercalation of nanoparticles, J. Appl. Phys. 107 (2010) 026104, https://doi.org/10.1063/1.3294960.
[31] S. Kumar, D. Parks, K. Kamrin, Mechanistic origin of the ultrastrong adhesion between graphene and a -SiO $_2$: beyond van der Waals, ACS Nano 10 (2016) 6552–6562, https://doi.org/10.1021/acsnano.6b00382.
[32] M. Ishigami, J.H. Chen, W.G. Cullen, M.S. Fuhrer, E.D. Williams, Atomic structure of graphene on SiO $_2$, Nano Lett. 7 (2007) 1643–1648, https://doi.org/10.1021/nl070613a.
[33] F.W. DelRio, M.P. de Boer, J.A. Knapp, E. David Reedy, P.J. Clews, M.L. Dunn, The role of van der Waals forces in adhesion of micromachined surfaces, Nat. Mater. 4 (2005) 629–634, https://doi.org/10.1038/nmat1431.
[34] B.E. Deal, M. Sklar, A.S. Grove, E.H. Snow, Characteristics of the surface-state charge (Qss) of thermally oxidized silicon, J. Electrochem. Soc. 114 (1967) 266–274 (accessed June 21, 2017), http://jes.ecsdl.org/content/114/3/266.short.
[35] B.M. Lowe, C.-K. Skylaris, N.G. Green, Acid-base dissociation mechanisms and energetics at the silica-water interface: an activationless process, J. Colloid Interface Sci. 451 (2015) 231–244, https://doi.org/10.1016/j.jcis.2015.01.094.
[36] S.M. Song, B.J. Cho, Investigation of interaction between graphene and dielectrics, Nanotechnology 21 (2010) 335706, https://doi.org/10.1088/0957-4484/21/33/335706.
[37] C. Casiraghi, S. Pisana, K.S. Novoselov, A.K. Geim, A.C. Ferrari, Raman fingerprint of charged impurities in graphene, Appl. Phys. Lett. 91 (2007) 233108, https://doi.org/10.1063/1.2818692.
[38] A. Das, S. Pisana, B. Chakraborty, S. Piscanec, S.K. Saha, U.V. Waghmare, K.S. Novoselov, H.R. Krishnamurthy, A.K. Geim, A.C. Ferrari, A.K. Sood, Monitoring dopants by Raman scattering in an electrochemically top-gated graphene transistor, Nat. Nanotechnol. 3 (2008) 210–215, https://doi.org/10.1038/nnano.2008.67.
[39] M. Kalbac, A. Reina-Cecco, H. Farhat, J. Kong, L. Kavan, M.S. Dresselhaus, The influence of strong electron and hole doping on the Raman intensity of chemical vapor-deposition graphene, ACS Nano 4 (2010) 6055–6063, https://doi.org/10.1021/nn1010914.
[40] S. Ryu, L. Liu, S. Berciaud, Y.-J. Yu, H. Liu, P. Kim, G.W. Flynn, L.E. Brus, Atmospheric oxygen binding and hole doping in deformed graphene on a SiO $_2$ substrate, Nano Lett. 10 (2010) 4944–4951, https://doi.org/10.1021/nl1029607.
[41] T.O. Wehling, K.S. Novoselov, S.V. Morozov, E.E. Vdovin, M.I. Katsnelson, A.K. Geim, A.I. Lichtenstein, Molecular doping of graphene, Nano Lett. 8 (2008) 173–177, https://doi.org/10.1021/nl072364w.
[42] S. Dou, A. Shen, L. Tao, S. Wang, Molecular doping of graphene as metal-free electrocatalyst for oxygen reduction reaction, Chem. Commun. 50 (2014) 10672, https://doi.org/10.1039/C4CC05055J.
[43] M.S. Abdou, F.P. Orfino, Z.W. Xie, M.J. Deen, S. Holdcroft, Reversible charge transfer complexes between molecular oxygen and poly(3-alkylthiophene)s, Adv. Mater. 6 (1994) 838–841 (accessed June 16, 2017), http://onlinelibrary.wiley.com/doi/10.1002/adma.19940061106/full.
[44] Y. ying Wang, Z. hua Ni, T. Yu, Z.X. Shen, H. min Wang, Y. hong Wu, W. Chen, A.T. Shen Wee, Raman studies of monolayer graphene: the substrate effect, J. Phys. Chem. C 112 (2008) 10637–10640, https://doi.org/10.1021/jp8008404.
[45] S. Das, D. Lahiri, A. Agarwal, W. Choi, Interfacial bonding characteristics between graphene and dielectric substrates, Nanotechnology 25 (2014) 045707, https://doi.org/10.1088/0957-4484/25/4/045707.
[46] Y.-J. Kang, J. Kang, K.J. Chang, Electronic structure of graphene and doping effect on SiO 2, Phys. Rev. B 78 (2008), https://doi.org/10.1103/PhysRevB.78.115404.
[47] Z. Cheng, Q. Zhou, C. Wang, Q. Li, C. Wang, Y. Fang, Toward intrinsic graphene surfaces: a systematic study on thermal annealing and wet-chemical treatment of SiO $_2$ -supported graphene devices, Nano Lett. 11 (2011) 767–771, https://doi.org/10.1021/nl103977d.
[48] J.E. Lee, G. Ahn, J. Shim, Y.S. Lee, S. Ryu, Optical separation of mechanical strain from charge doping in graphene, Nat. Commun. 3 (2012) 1024, https://doi.org/10.1038/ncomms2022.
[49] N.S. Mueller, S. Heeg, M.P. Alvarez, P. Kusch, S. Wasserroth, N. Clark, F. Schedin, J. Parthenios, K. Papagelis, C. Galiotis, M. Kalbáč, A. Vijayaraghavan, U. Huebner, R. Gorbachev, O. Frank, S. Reich, Evaluating arbitrary strain configurations and doping in graphene with Raman spectroscopy, 2D Mater. 5 (2017) 015016, https://doi.org/10.1088/2053-1583/aa90b3.
[50] A. Das, B. Chakraborty, S. Piscanec, S. Pisana, A.K. Sood, A.C. Ferrari, Phonon renormalization in doped bilayer graphene, Phys. Rev. B 79 (2009), https://doi.org/10.1103/PhysRevB.79.155417.
[51] G. Froehlicher, S. Berciaud, Raman spectroscopy of electrochemically gated graphene transistors: geometrical capacitance, electron-phonon, electron-electron, and electron-defect scattering, Phys. Rev. B 91 (2015), https://doi.org/10.1103/PhysRevB.91.205413.
[52] Y.-J. Kang, J. Kang, K.J. Chang, Electronic structure of graphene and doping effect on SiO 2, Phys. Rev. B 78 (2008), https://doi.org/10.1103/PhysRevB.78.115404.
[53] M.M. Fogler, D.S. Novikov, B.I. Shklovskii, Screening of a hypercritical charge in graphene, Phys. Rev. B 76 (2007), https://doi.org/10.1103/PhysRevB.76.233402.
[54] L. Bousse, N.F. De Rooij, P. Bergveld, Operation of chemically sensitive field-effect sensors as a function of the insulator-electrolyte interface, IEEE Trans. Electron Devices 30 (1983) 1263–1270.
[55] C.D. Fung, P.W. Cheung, W.H. Ko, A generalized theory of an electrolyte-insulator-semiconductor field-effect transistor, IEEE Trans. Electron Devices 33 (1986) 8–18.
[56] M. Nonnenmacher, M.P. O'Boyle, H.K. Wickramasinghe, Kelvin probe force microscopy, Appl. Phys. Lett. 58 (1991) 2921–2923, https://doi.org/10.1063/1.105227.
[57] V. Panchal, R. Pearce, R. Yakimova, A. Tzalenchuk, O. Kazakova, Standardization of surface potential measurements of graphene domains, Sci. Rep. 3 (2013), https://doi.org/10.1038/srep02597.
[58] A.K. Henning, T. Hochwitz, J. Slinkman, J. Never, S. Hoffmann, P. Kaszuba, C. Daghlian, Two-dimensional surface dopant profiling in silicon using scanning Kelvin probe microscopy, J. Appl. Phys. 77 (1995) 1888–1896, https://doi.org/10.1063/1.358819.
[59] C. Maragliano, S. Lilliu, M.S. Dahlem, M. Chiesa, T. Souier, M. Stefancich, Quantifying charge carrier concentration in ZnO thin films by Scanning Kelvin Probe Microscopy, Sci. Rep. 4 (2015), https://doi.org/10.1038/srep04203.
[60] W.N. Hansen, G.J. Hansen, Standard reference surfaces for work function measurements in air, Surf. Sci. 481 (2001) 172–184, https://doi.org/10.1016/S0039-6028(01)01036-6.
[61] O.A. Castañeda-Uribe, R. Reifenberger, A. Raman, A. Avila, Depth-sensitive subsurface imaging of polymer nanocomposites using second harmonic Kelvin probe force microscopy, ACS Nano 9 (2015) 2938–2947, https://doi.org/10.1021/nn507019c.
[62] D. Pierucci, J.-J. Gallet, F. Bournel, F. Sirotti, M.G. Silly, H. Tissot, A. Naitabdi, F. Rochet, Real-time X-ray photoemission spectroscopy study of Si(001)-2×1 exposed to water vapor: adsorption kinetics, Fermi level positioning, and electron affinity variations, J. Phys. Chem. C 120 (2016) 21631–21641, https://doi.org/10.1021/acs.jpcc.6b07360.
[63] W. Mönch, Hydrogen-modification of electronic surface, bulk, and interface properties of Si, Phys. Status Solidi A 159 (1997) 25–37, https://doi.org/10.1002/1521-396X(199701)159:1<25::AID-PSSA25>3.0.CO;2-C.
[64] T. Hattori, Advanced Research Workshop on Fundamental Aspects of Ultrathin Dielectrics on Si-Based Devices: towards an Atomic-Scale Understanding, 1998.
[65] T. Hattori, Surface, interface and valence band structures of ultra-thin silicon oxides, Appl. Surf. Sci. 130–132 (1998) 156–164, https://doi.org/10.1016/S0169-4332(98)00043-9.
[66] H. Nohira, A. Omura, M. Katayama, T. Hattori, Valence band edge of ultra-thin silicon oxide near the interface, Appl. Surf. Sci. 123–124 (1998) 546–549, https://doi.org/10.1016/S0169-4332(97)00568-0.
[67] P.V. Avramov, A.A. Kuzubov, A.S. Fedorov, P.B. Sorokin, F.N. Tomilin, Y. Maeda, Density-functional theory study of the electronic structure of thin Si ⁄ Si O 2 quantum nanodots and nanowires, Phys. Rev. B 75 (2007), https://doi.org/10.1103/PhysRevB.75.205427.

Supporting Information

Investigation of charges-driven interaction between graphene and different SiO_2 surfaces

*Maria F. Pantano[1], Erica Iacob[2], Antonino Picciotto[2], Benno Margesin[2], Alba Centeno[3], Amaia Zurutuza[3],Costas Galiotis[4,5], Nicola M. Pugno[1,6,7**], Giorgio Speranza[2,8,9*]*

[1]Laboratory of Bio-inspired & Graphene Nanomechanics, Department of Civil, Environmental and Mechanical Engineering, University of Trento, Via Mesiano 77, 38123 Trento, Italy

[2]Centre for Materials and Microsystems, Fondazione Bruno Kessler, Via Sommarive 18, 38123 Povo (TN), Italy

[3]GRAPHENEA S.A. Paseo Mikeletegi 83, 20009, San Sebastian, Spain

[4]Institute of Chemical Engineering Sciences, Foundation for Research and Technology – Hellas (FORTH/ICE-HT), Patras 265 04, Greece

[5]Department of Chemical Engineering, University of Patras, Patras 26504, Greece

[6]School of Engineering and Materials Science, Queen Mary University of London, Mile End Road, London E1 4NS, U.K.

[7]Ket-Lab, Edoardo Amaldi Foundation, Via del Politecnico snc, 00133 Rome, Italy

[8]Istituto Fotonica e Nanotecnologie – CNR, via alla cascata 56, 38123 Trento, Italy

[9]Department of Material Engineering, University of Trento, Via Mesiano 77, 38123 Trento, Italy

Sample preparation

A set of 7 different Silicon based substrates was produced:

1) Silicon with 111 orientation with on top 300 nm oxide grown through direct oxidation of underlying Si (thermal oxide);

**nicola.pugno@unitn.it;

* speranza@fbk.eu

2) Silicon with 111 orientation with on top 300 nm oxide deposited using tetraethylorthosilicate (TEOS) as silicon oxide precursor;

3) Silicon with 111 orientation with on top 300 nm TEOS annealed at 950°C for 30 minutes after TEOS deposition;

4) Silicon with 111 orientation with 300 nm thermal oxide annealed at 950° for 30 minutes after oxide growth;

5) HF etched silicon with 111 orientation with a film of CH_4+H_2 on top;

6) Silicon with 111 orientation with only native oxide;

7) Quartz with no crystal orientation.

Raman analysis

It is known that any modification of the electric charge in a system of atoms leads to softening or stiffening of the phonon modes [1],[2], which induces changes to the G and 2D band positions and intensity. As an example, it is known that bonding of C atoms with H atoms induces the formation of a gap with a consequent transition from graphene to graphane [3]. In Raman spectra this corresponds to the appearance of the D, D' and D+D' bands. Different is the case of fluoro-graphene where the 2D band progressively disappears with an increasing fluorination degree, which, as a limit condition, causes the Raman spectrum to appear as that of GO [4]. Concerning oxygen, it has been demonstrated that oxygen molecules adsorbed on a SiO_2 surface may inject charges in graphene [5]. Oxygen and charged molecular species are in fact able to interact with the aromatic rings of graphene modifying its charge distribution [6], [7], [8]. All these considerations suggest that a different preparation of the SiO_2 surface of our samples should determine detectable changes in the Raman spectra of monolayer graphene depending on the strength of its interaction with the substrate.

Our Raman measurements were carried out with a 632.8 nm laser at a magnification of 50x and a 1200 grooves/mm grating. Spectra were acquired with an integration time of 5s repeated twenty times. The data reported refer to the mean of 6 measurements at different locations on the same sample. Before the analysis, all the samples were cleaned by thermal annealing at 500°C for 1h with the only exception of Si covered with CH_4+H_2, which would be destroyed by such high temperature. The acquired Raman spectra (Figure S1) were then processed with open-source *fityk* software, which allowed us to identify all their main features (summarized in Table S1).

Table S1. Summary of the main features characterizing the Raman spectra of graphene transferred on top of 7 different Si/SiO_2 substrates.

Substrate	G peak			2D peak			I(G)/I(2D)
	Position [cm^{-1}]	Height [counts]	FWHM [cm^{-1}]	Position [cm^{-1}]	Height [counts]	FWHM [cm^{-1}]	
TO	1611 ± 1	97 ± 14	6.4 ± 0.9	2661 ± 1	123 ± 13	17.1 ± 0.5	1.28 ± 0.07
TO+AN	1604 ± 2	518 ± 110	6.9 ± 1.0	2656 ± 1	375 ± 66	15.9 ± 0.6	0.74 ± 0.14
NO	1604.2 ± 0.5	230 ± 219	6.6 ± 0.4	2654 ± 1	166 ± 235	18.8 ± 1.0	1.00 ± 0.51
Quartz	1603 ± 1	137 ± 13	7.0 ± 0.9	2653 ± 2	162 ± 14	16.8 ± 0.8	1.18 ± 0.02
TEOS	1597 ± 1	288 ± 8	10.9 ± 0.2	2638 ± 1	244 ± 12	24. 0 ± 0.3	0.85 ± 0.04
TEOS+AN	1593 ± 2	345 ± 44	11.2 ± 0.6	2638 ± 5	312 ±71	23.2 ± 1.4	0.90 ± 0.15
CH_4+H_2	1585 ± 5	296 ± 286	9.8 ± 2.2	2643 ± 9	440 ± 366	20. 2 ± 2.2	1.65 ± 0.76

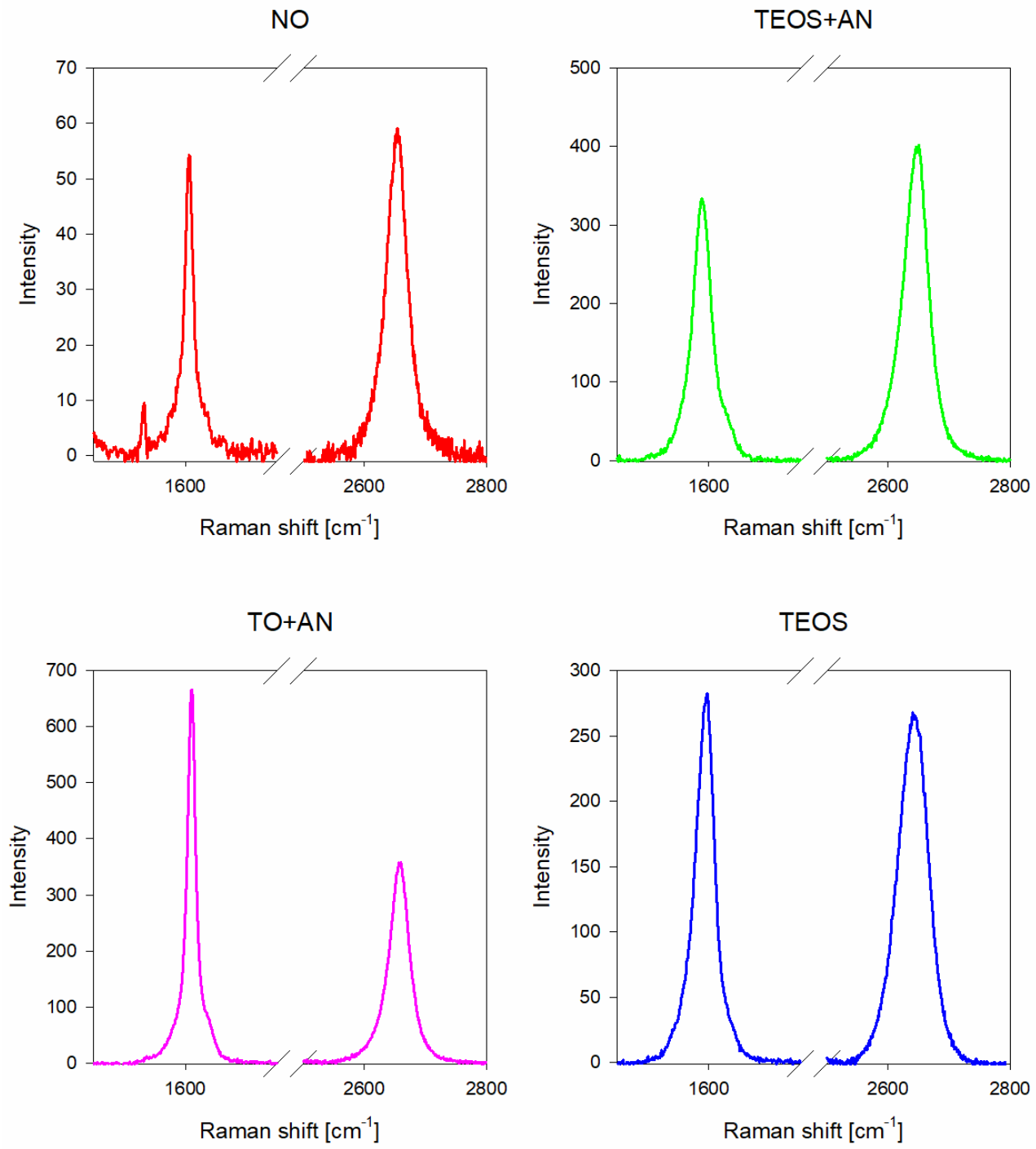

Figure S1: Raman spectra acquired for example Si substrates with native oxide (NO), TEOS oxide, annealed TEOS oxide (TEOS+AN) and annealed thermal oxide (TO+AN) on top.

Computation of the strain and charge in graphene samples

From the G – 2D frequencies plot (Figure S2), we can derive both the amount of strain and charge affecting our graphene samples. In particular, as the regression line (dashed in Figure S2)

representing our samples results to be reasonably parallel (slope: 0.89) to the reference line corresponding to zero strain samples (slope: 0.75 ± 0.04 [9]), we can assume that no significant variation in strain affects our samples. We can then derive the amount of strain according to the following procedure. First, for each point representing our samples we can draw a line *l* parallel to the free strain line. The intersection between *l* and the free charge line defines a new point P*, which results to have the following G frequency, ω_G*:

$$\omega_G^* = -\frac{q^{0C} - q^l}{m^{0C} - m^l} \tag{1}$$

where m^{0C} (equal to 2.2[9]) and q^{0C} (equal to -802.62 cm^{-1}) are the slope and the intercept of the zero charge line, respectively, and m^l and q^l are the slope and the intercept of the line *l*. While m^l is always equal to 0.75, q^l depends on the specific sample point we are considering.

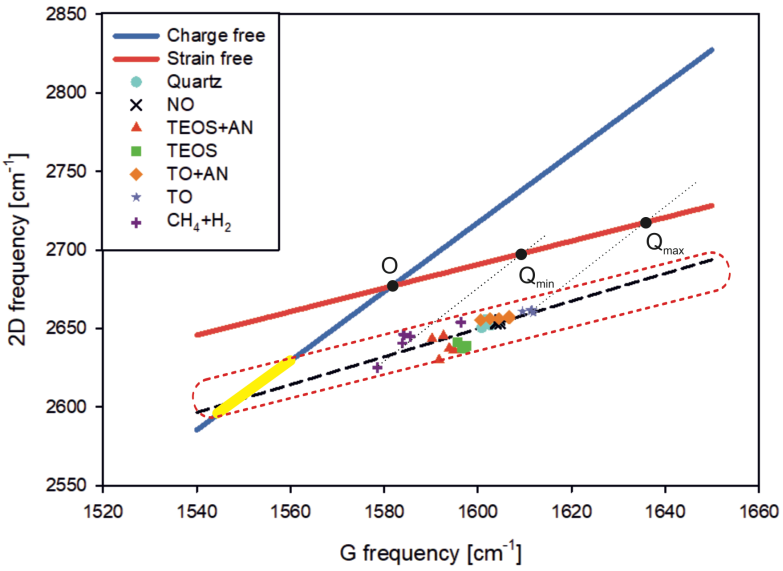

Figure S2: Frequency of the 2D peak vs the frequency of the G peak of a monolayer graphene deposited on different silicon substrates. The experimental points are aligned almost parallel to the reference line corresponding to a graphene sample with no strain. The yellow region of the free charge line allows to estimate the strain interval across our samples. The highlighted points Q_{min} and Q_{max} allow for the evaluation the minimum and maximum charge affecting our graphene samples deposited on different Si substrates.

The G frequency of P* is shifted from the reference point $O \equiv (1581.6; 2676.9)$ cm^{-1} by $\Delta\omega_G = \omega_G^* - \omega_0$ (see Figure S2). Then $\Delta\omega_G$ allows to estimate the corresponding hydrostatic strain, ε_h, as [10] :

$$\varepsilon_h = - \Delta\omega_G / \omega_0 \gamma \quad (2)$$

where ω_0 is the G frequency of the reference point and γ is the Grüeneisen parameter equal to 1.8 [10]. As the above mentioned procedure can be repeated for each of our samples, we can determine a set of P* points (yellow region of the free charge line) each corresponding to a value of the hydrostatic strain. The resulting hydrostatic strain $\varepsilon_h = \varepsilon_{xx} + \varepsilon_{yy}$ is 1.0% ± 0.1% (Table S2). As our graphene samples are polycrystalline with arbitrary orientation of the crystallites, it reasonable to assume that an equal strain is applied along two orthogonal directions x and y, i.e. $\varepsilon_{xx} = \varepsilon_{yy} = 0.5\%$.

Table S2. Evaluation of the strain and charge density of graphene sheets transferred on top of 7 different Si/SiO_2 substrates. Data derived from the analysis of Raman spectra.

Substrate	Strain estimation (%)	Charge density ($\cdot 10^{13}$ cm^{-2})
TO	0.91%	4.17
	0.92%	4.21
	0.91%	4.20
	0.96%	4.31
	0.90%	4.02
TO+AN	0.94%	3.90
	0.88%	3.46
	0.92%	3.69
	0.92%	3.85
	0.87%	3.28
NO	0.94%	3.75
	0.99%	3.86
	0.99%	3.78
	0.97%	3.74
	0.97%	3.73
Quartz	0.99%	3.56
	0.94%	3.67
	0.88%	3.38
	0.98%	3.79
	0.99%	3.71
TEOS	1.13%	3.47
	1.22%	3.75
	1.24%	3.82
	1.23%	3.81
	1.21%	3.78

TEOS+AN	0.97% 1.19% 1.23% 1.32% 0.97%	2.90 3.46 3.62 3.59 2.71
CH_4+H_2	0.79% 0.80% 1.20% 0.92% 0.83% 0.85%	1.87 1.91 2.34 2.13 2.88 2.12

The presence of strain in graphene samples can be related to the friction caused by water slippage on graphene during its wet transfer on a Si wafer. The friction force, F_f, due to the motion of graphene in water, can be evaluated as [11]:

$$F_f = \lambda v_{slip} A \tag{3}$$

Where F_f, is parallel to the graphene sheet, A is the area of the graphene sheet (equal to 15 mm^2 in the case of our experiments), λ is the friction coefficient, which is equal to $9.6 \cdot 10^4$ Ns/m^3 [11] for friction between water and graphene, and v_{slip} is the velocity jump at the graphene/water interface. During a typical wet transfer process the water layer beneath a graphene sample is provided with a velocity of few mm/s due to approaching of a Si substrate. It is reasonable to assume v_{slip}=5mm/s, then from equation 3 it follows that the friction force experienced by our graphene samples during wet transfer is 7.7 mN. If we consider that the Young's modulus of graphene, E, is 1 TPa [12], the friction force can cause the graphene sample to undergo a strain, ε, equal to: $\varepsilon = F_f/(E \cdot w \cdot t)$, where w and t are respectively the width (3 - 4 mm) and thickness (0.335 nm) of the graphene sample. Overall, this results in a strain of 0.54% - 0.72%. Note that due to the simplicity of the analytical approach these are to be intended as purely indicative values. Nevertheless, they are in good agreement with the estimation derived from the analysis of the Raman spectra.

From the analysis of Raman spectra and with the same approach considered before, we can also derive the amount of charge in our samples. Let us first consider the dataset corresponding to graphene on Si with TO on top, which shows the most blue-shifted 2D frequency. Let us compute the line parallel to the zero charge reference line that crosses the point with the highest 2D frequency, which is (1611.6; 2661.7) cm^{-1} (grey dotted line in figure S2). Such line has slope equal to 2.2 and intercept equal to -883.74 cm^{-1}. Then, again by the means of equation 1, we can identify the intersection point Q_{max} between such newly computed line and the reference zero strain line (that has slope, m^{0S}, equal to 0.75 and intercept, q^{0S}, equal to 1490.7 cm^{-1}). The intersection point, Q_{max}, results to be (1637.54; 2718.86) cm^{-1}. Since the sensitivity of the 2D frequency to the charge per unit area, $\Delta\omega_{2D}/\Delta n$, is about 10^{-12} cm^2/cm [9], we can derive that our samples are affected by an electric charge per unit area of (2718.9-2676.9) cm^{-1}/ 10^{-12} $cm^2/cm \approx 42 \cdot 10^{12}$ cm^{-2}. We can now repeat the same procedure for each data point (Table S2). If we consider the sample with the least blue-shifted 2D frequency, this is identified by (1578.56; 2624.94) cm^{-1} in the G-2D frequencies plane and corresponds to a graphene sheet deposited on Si with a CH_4+H_2 layer. The charge amount corresponding to this sample is $\approx 23 \cdot 10^{12}$ cm^{-2}. In summary, the charge affecting our samples vary within the interval $23\text{-}42 \cdot 10^{12}$ cm^{-2}.

Scanning Kelvin Probe Microscopy

The images were acquired with an Atomic Force Microscope (AFM) named Solver Px by NT-MDT. AFM topographical data were acquired in semi-contact mode meanwhile surface potential was measured using Amplitude Modulation-Scanning Kelvin Probe Microscopy (SKPM or KPFM).

Kelvin mode is based on a two-pass technique[13]. In the first pass the topography is acquired using standard semicontact mode (mechanical excitation of the cantilever), from which we can estimate the surface roughness (Table S3). In the second pass the tip is kept at a fixed distance (10 nm) from

the surface and previous topography is retraced in order to detect the electric surface potential. During this second pass the cantilever is no longer excited mechanically but electrically.

Table S3: Arithmetical mean roughness (R_a) and root mean square roughness (R_q) of different SiO_2 surfaces measured by AFM.

Sample	R_a [nm]	R_q [nm]
TO	0.2	0.4
TO+AN	0.4	0.6
NO	0.6	0.8
Quartz	1.4	3.4
TEOS	0.9	1.1
TEOS+AN	0.8	1.1
CH_4+H_2	0.2	0.5

X-ray Photoelectron Spectroscopy (XPS)

The position of the Valence Band (VB) top can be estimated following two methods: the first one is a conventional method, based on the intersection between a linear fitting on the falling shoulder of the VB and the VB background above the Fermi level. The data reported in the main text were derived according to this method. Alternatively, the VB-top can be estimated from a threshold calculated as a fraction of the integral intensity of the VB after background subtraction.

Figure S3 shows a comparison between the VB-top estimations derived from both methods. The good agreement between them assesses the significance of our results.

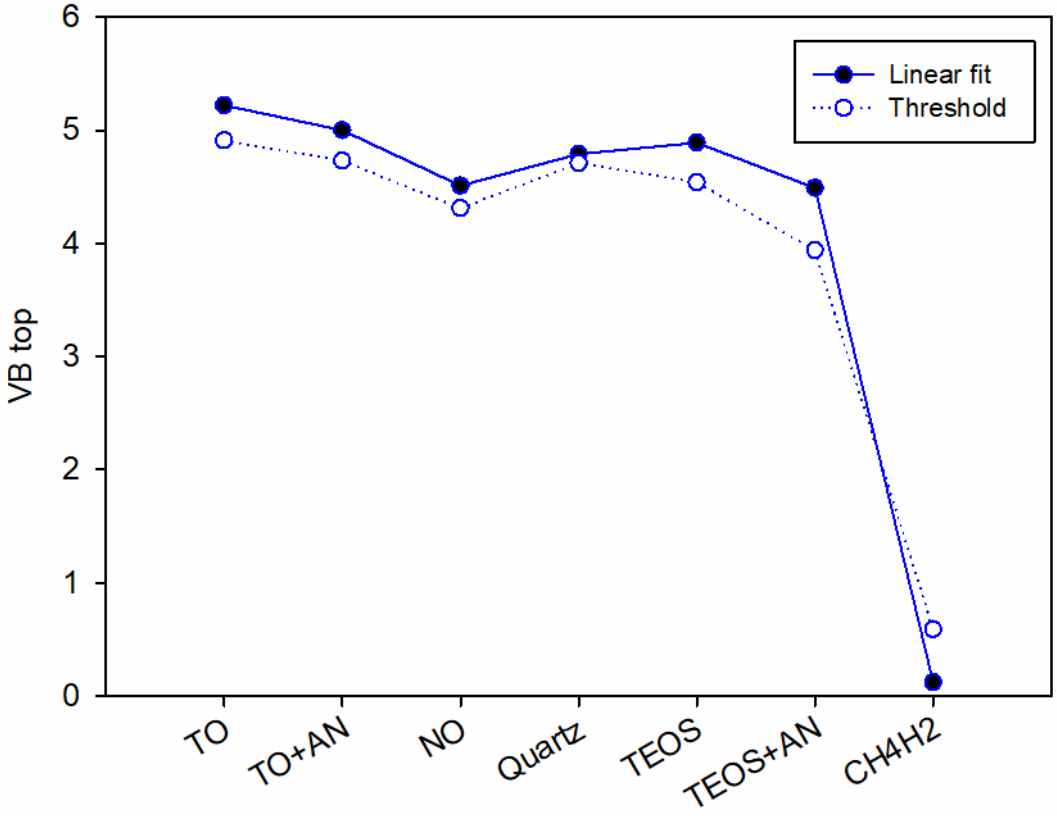

Figure S3: Comparison between the Valence Band (VB) top found for different Si-based substrates according to two alternative methods. In the first case (conventional method), the VB-top is determined as the intersection between the linear fittings on the falling shoulder of the VB and the VB background above the Fermi level. In the second case, the VB top can be estimated utilizing a threshold calculated as a fraction of the integral intensity of the VB after background subtraction.

In the case of sample with native oxide, the procedure was slightly modified in order to eliminate the contribution of the bulk Si substrate. Initially, after linear background subtraction, the VB was fitted with a number of Gaussian components as shown in figure S4. Then, following the interpretation given by Hattori in [14], the contribution of the bulk Si substrate was eliminated suppressing the feature proximal to the Fermi edge. The result is shown in figure S4b where the SiO_2 valence band is modeled using 5 Gaussian components.

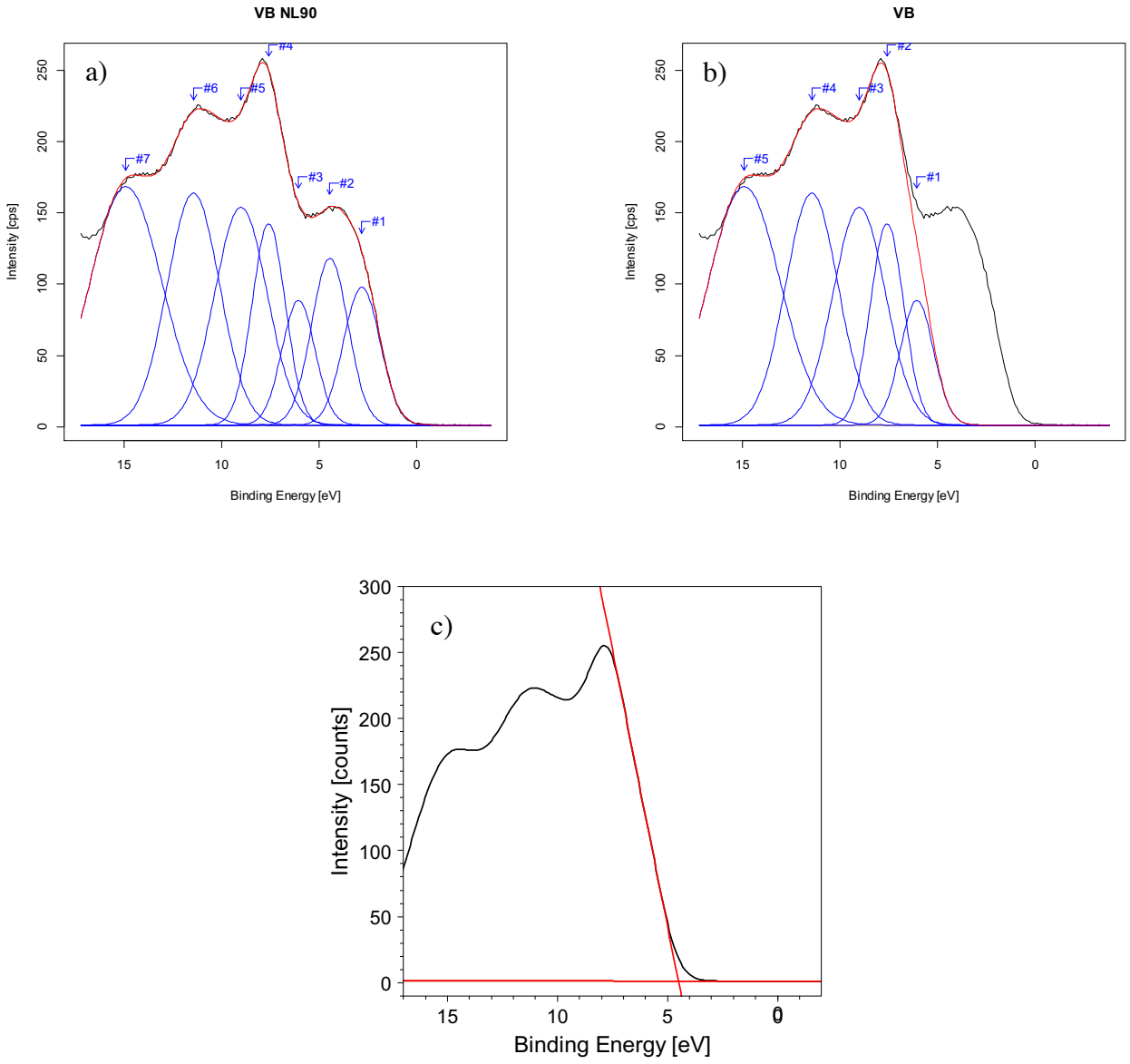

Figure S4: (a) Gaussian fit of the valence band of a SiO_2/Si system; (b) Gaussian model of the NO VB after subtraction of the contribution of the bulk Si; (c) estimation of the VB-top using the linear fit.

The VB top is then evaluated applying a linear fit to the falling and flat branches of the VB, resulting in a value of 4.51eV in very good agreement with data reported in [14].

Supplementary References

[1] C. Casiraghi, S. Pisana, K.S. Novoselov, A.K. Geim, A.C. Ferrari, Raman fingerprint of charged impurities in graphene, Appl. Phys. Lett. 91 (2007) 233108. doi:10.1063/1.2818692.

[2] A. Das, S. Pisana, B. Chakraborty, S. Piscanec, S.K. Saha, U.V. Waghmare, K.S. Novoselov, H.R. Krishnamurthy, A.K. Geim, A.C. Ferrari, A.K. Sood, Monitoring dopants by Raman scattering in an electrochemically top-gated graphene transistor, Nat. Nanotechnol. 3 (2008) 210–215. doi:10.1038/nnano.2008.67.

[3] D.C. Elias, R.R. Nair, T.M.G. Mohiuddin, S.V. Morozov, P. Blake, M.P. Halsall, A.C. Ferrari, D.W. Boukhvalov, M.I. Katsnelson, A.K. Geim, K.S. Novoselov, Control of Graphene's Properties by Reversible Hydrogenation: Evidence for Graphane, Science. 323 (2009) 610–613. doi:10.1126/science.1167130.

[4] R.R. Nair, W. Ren, R. Jalil, I. Riaz, V.G. Kravets, L. Britnell, P. Blake, F. Schedin, A.S. Mayorov, S. Yuan, M.I. Katsnelson, H.-M. Cheng, W. Strupinski, L.G. Bulusheva, A.V. Okotrub, I.V. Grigorieva, A.N. Grigorenko, K.S. Novoselov, A.K. Geim, Fluorographene: A Two-Dimensional Counterpart of Teflon, Small. 6 (2010) 2877–2884. doi:10.1002/smll.201001555.

[5] S. Ryu, L. Liu, S. Berciaud, Y.-J. Yu, H. Liu, P. Kim, G.W. Flynn, L.E. Brus, Atmospheric Oxygen Binding and Hole Doping in Deformed Graphene on a SiO_2 Substrate, Nano Lett. 10 (2010) 4944–4951. doi:10.1021/nl1029607.

[6] T.O. Wehling, K.S. Novoselov, S.V. Morozov, E.E. Vdovin, M.I. Katsnelson, A.K. Geim, A.I. Lichtenstein, Molecular Doping of Graphene, Nano Lett. 8 (2008) 173–177. doi:10.1021/nl072364w.

[7] S. Dou, A. Shen, L. Tao, S. Wang, Molecular doping of graphene as metal-free electrocatalyst for oxygen reduction reaction, Chem. Commun. 50 (2014) 10672. doi:10.1039/C4CC05055J.

[8] M.S. Abdou, F.P. Orfino, Z.W. Xie, M.J. Deen, S. Holdcroft, Reversible charge transfer complexes between molecular oxygen and poly(3-alkylthiophene)s, Adv. Mater. 6 (1994) 838–841. http://onlinelibrary.wiley.com/doi/10.1002/adma.19940061106/full (accessed June 16, 2017).

[9] J.E. Lee, G. Ahn, J. Shim, Y.S. Lee, S. Ryu, Optical separation of mechanical strain from charge doping in graphene, Nat. Commun. 3 (2012) 1024. doi:10.1038/ncomms2022.

[10] N.S. Mueller, S. Heeg, M.P. Alvarez, P. Kusch, S. Wasserroth, N. Clark, F. Schedin, J. Parthenios, K. Papagelis, C. Galiotis, M. Kalbáč, A. Vijayaraghavan, U. Huebner, R. Gorbachev, O. Frank, S. Reich, Evaluating arbitrary strain configurations and doping in graphene with Raman spectroscopy, 2D Mater. 5 (2017) 015016. doi:10.1088/2053-1583/aa90b3.

[11] G. Tocci, L. Joly, A. Michaelides, Friction of Water on Graphene and Hexagonal Boron Nitride from *Ab Initio* Methods: Very Different Slippage Despite Very Similar Interface Structures, Nano Lett. 14 (2014) 6872–6877. doi:10.1021/nl502837d.

[12] C. Lee, X. Wei, J.W. Kysar, J. Hone, Measurement of the Elastic Properties and Intrinsic Strength of Monolayer Graphene, Science. 321 (2008) 385–388. doi:10.1126/science.1157996.

[13] M. Nonnenmacher, M.P. O'Boyle, H.K. Wickramasinghe, Kelvin probe force microscopy, Appl. Phys. Lett. 58 (1991) 2921–2923. doi:10.1063/1.105227.

[14] T. Hattori, Surface, interface and valence band structures of ultra-thin silicon oxides, Appl. Surf. Sci. 130–132 (1998) 156–164. doi:10.1016/S0169-4332(98)00043-9.

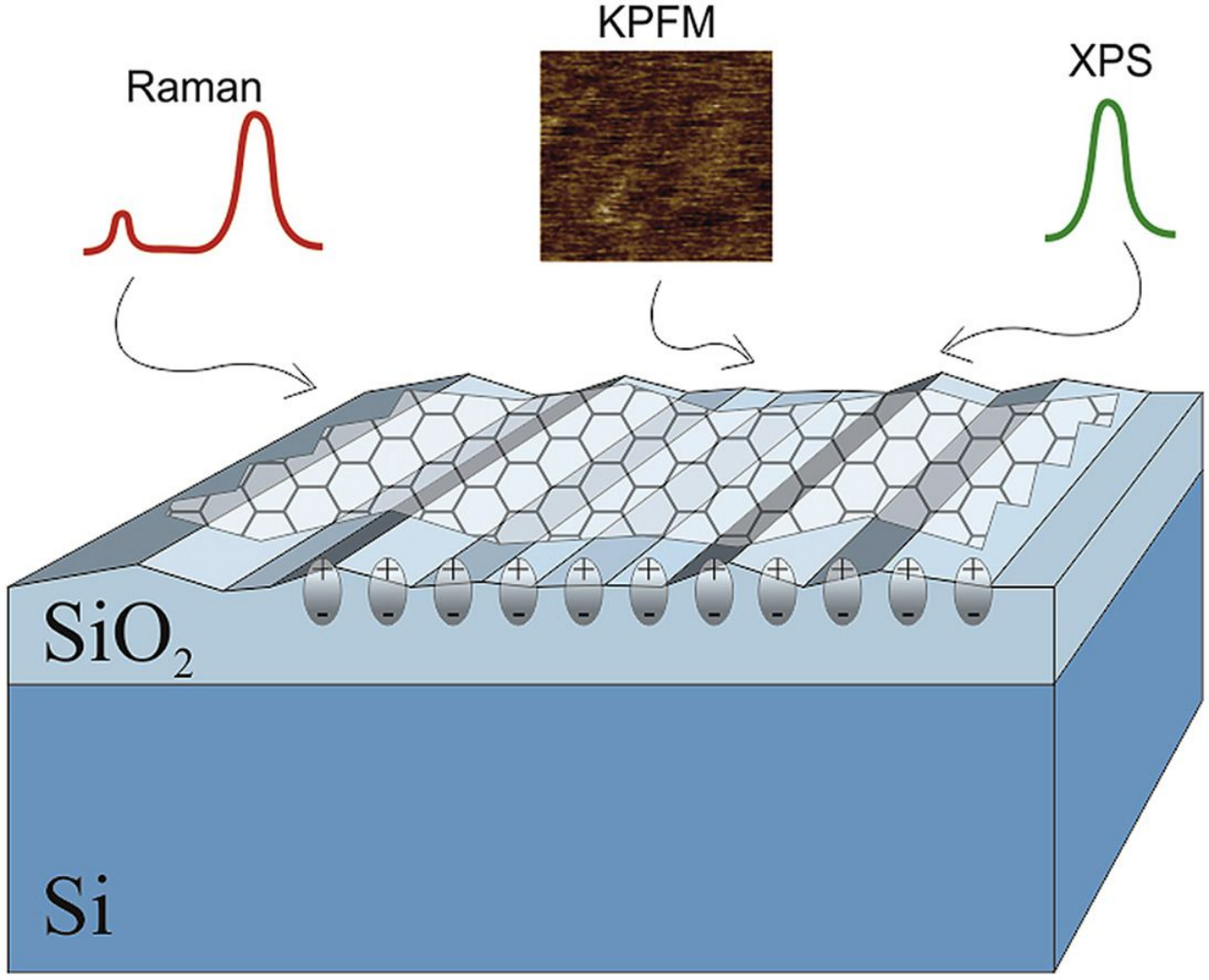
KPFM
Raman
XPS
SiO2
Si